Research Square

Preprints are preliminary reports that have not undergone peer review.
They should not be considered conclusive, used to inform clinical practice,
or referenced by the media as validated information.

Phylogenetic and Genomic Analysis of Multi-resistance in Salmonella Enterica

Stuart Ngereza
stuartngereza5@gmail.com

Genomac Institute
Jemimah Ogwerel
Genomac Institute https://orcid.org/0009-0003-7601-226X
Taye Motunrayo Ilesanmi
Genomac Institute
Sefi Omole Ijeboi
Genomac Institute
Godspower Oluwatomilade Akinmade
Genomac Institute

Research Article

Keywords: Salmonella enterica, multidrug resistance, antimicrobial resistance, Africa

Posted Date: September 16th, 2026

DOI: https://doi.org/10.21203/rs.3.rs-10878139/v1

License: This work is licensed under a Creative Commons Attribution 4.0 International License. Read Full License

Additional Declarations: The authors declare no competing interests.

Abstract

Salmonella enterica is a severe global foodborne pathogen facing intense evolutionary pressures from the unregulated use of conventional antibiotics and widespread exposure to non-antibiotic antibacterials, such as biocides and heavy metals. This chemical overlap drives the co-selection and maintenance of multidrug-resistant (MDR) strains. This study investigates how phylogenetic relationships shape the distribution and evolution of the genomic determinants responsible for multidrug and cross-resistance across diverse African lineages. The analysis examined 20 *S. enterica* genomes retrieved from the NCBI Pathogen Detection database. These isolates represent broad geographic and epidemiological diversity across Africa, originating from clinical specimens, food animals, and food products. Bioinformatic workflows included genome annotation via BV-BRC, biocide and heavy metal resistance screening against the BacMet database, whole-genome single-nucleotide polymorphism (SNP) calling using Snippy, maximum-likelihood phylogenetic reconstruction via IQ-TREE, and pangenome comparative analysis. The genomic architecture of resistance in these African isolates is actively shaped by regional phylogenetic relationships, anthropogenic co-selection, and intricate efflux system regulation. Phylogenetic clustering indicated active cross-border transmission of ancestral lineages. Notably, the AcrEF-TolC system unexpectedly dominated the typically ubiquitous AcrAB-TolC pump as the primary mechanism associated with ciprofloxacin resistance. The data further demonstrated that environmental exposure to common biocides (such as triclosan and quaternary ammonium compounds) and industrial heavy metals (such as gold and zinc) explicitly co-selects for clinical antibiotic resistance. Finally, resistance profiles were highly decoupled from core genomic phylogeny, indicating that rapid, localized horizontal gene transfer of accessory mobile elements heavily influences the resistance landscape. Multidrug resistance in African *S. enterica* is a complex byproduct of vertical evolutionary history, regulatory adaptation, and significant environmental co-selection. Combating this threat requires a unified One Health approach prioritizing regional genomic surveillance, the regulation of environmental heavy metal and biocide discharge, and reinforced antimicrobial stewardship.

BACKGROUND

Salmonella enterica is a highly diverse, Gram-negative pathogen responsible for a severe global burden of foodborne illness, manifesting clinically as enteric fever, acute gastroenteritis, and life-threatening bacteremia (Han et al., 2024). Within the species, S. enterica subspecies enterica (subspecies I) holds the greatest clinical significance, encompassing over 1,580 serovars capable of colonizing warm-blooded hosts and driving systemic infections in humans and livestock (Mkangara, 2023). The widespread, often unregulated use of conventional antibiotics in both human medicine and animal husbandry has accelerated the emergence of multidrug-resistant (MDR) Salmonella strains, severely compromising classical first-line and critically important treatment options worldwide.

Beyond traditional antibiotics, modern industrial and agricultural environments expose bacteria to non-antibiotic antibacterials (NAAs), including biocides (disinfectants and sanitizers) and heavy metals utilized as growth promoters or environmental contaminants. This chemical overlap creates a distinct evolutionary pressure: the co-selection of resistance. Genetic determinants encoding resistance to heavy metals (such as gold, copper, or arsenic) and biocides (such as quaternary ammonium compounds) are frequently co-located on mobile genetic elements or shared efflux pump regulatory systems alongside antibiotic resistance genes (Wand & Sutton, 2022). Consequently, exposure to environmental heavy metals can indirectly select for and maintain antibiotic-resistant phenotypes, even in the absence of active antibiotic deployment.

The complex interplay between genomic architecture, phylogenetic relationships, and these cross-resistance phenotypes remains poorly defined, particularly within the African continent. Despite the high endemic burden of salmonellosis in Africa, high-resolution genomic data characterizing how localized lineages evolve, mobilize, or maintain these overlapping resistance structures is historically underrepresented. Understanding these evolutionary pathways requires a robust integration of single-nucleotide polymorphism (SNP) phylogenetics with comprehensive pan-genomic resistome profiling.

Accordingly, this study aims to investigate how phylogenetic relationships shape the distribution and evolution of genomic determinants of multidrug and cross-resistance in Salmonella enterica. By integrating genomic characterization with evolutionary analysis using bioinformatic tools, we evaluate the co-occurrence of resistance to antibiotics and non-antibiotic antibacterials (NAAs) across diverse African lineages to provide critical baseline data for regional epidemiological surveillance.

METHODOLOGY

Data retrieval

A total of 20 Salmonella strains were retrieved from the NCBI Pathogen Detection database (https://www.ncbi.nlm.nih.gov/pathogens/). Associated metadata, including BioProject accession numbers, assembly accessions, strain identifiers, and project numbers, were collected and are summarised in Table 1. Most of the genomes were generated using the Illumina sequencing platform, producing high-quality short-read data. The isolates originated from multiple African countries, enabling a geographically diverse representation of Salmonella strains.

Table 1
Salmonella enterica Strain Information

Bioproject	Bio Sample	SRA	Strain ID	Size (MB)	Region	Isolation Source	Year	Platform	Assembly
PRJNA338674	SAMN03576807	SRR4733852	IOOPHAI16755	308.6	Tanzania	Feces	2019	Illumina	GCA_006921895.1
PRJNA275961	SAMN03576801	SRR8980099	CFSAN031267	319.0	Tanzania	Carcass	2019	Illumina	GCA_005903625.1
PRJEB56537	SAMEA11453912	ERR10359958	19CS0293	326.1	Nigeria	Clinical	2022	Illumina	GCA_027054895.1
PRJEB38609	SAMEA6669842	ERR4183562	D7	376.4	Nigeria	Poultry farms	2022	Illumina	GCA_023071015.1
PRJNA275962	SAMN02133632	SRR34721570	D1	506.7	South Africa	Poultry	2025	Illumina	GCA_051683645.1
PRJNA39546	SAMEA11553290	ERR12997065	YA00509485	325.4	South Africa	Human stool	2024	Illumina	GCA_043373295.1
PRJNA186035	SAMN13527237	SRR10665536	CFSAN072816	376.2	Tunisia	Clam	2020	Illumina	GCA_010576265.1
PRJNA186035	SAMN33428	SRR23603314	101	317.7	Tunisia	Bovine faeces	2023	Illumina	GCA_028850995.1
PRJEB2059669	SAMEA788792	ERR023769	A13198	347.1	Malawi	Blood	2020	Illumina	GCA_012169695.1
PRJEB2059	SAMEA788815	ERR029251	Q23F2_BM	316.4	Malawi	Bone marrow	2020	Illumina	GCA_010195165.1
PRJNA275961	SAMN03577106	SRR3133033	CFSAN031573	449.0	Ethiopia	Rumen	2019	Illumina	GCA_007757115.1
PRJEB634	SAMEA2053616	ERR311307	ILBSalm5484212	365.8	Uganda	Feces	2019	Illumina	GCA_009620335.1
PRJEB634	SAMEA2053416	ERR311308	ILBSalm5484214	365.4	Uganda	Blood	2019	Illumina	GCA_009628755.1
PRJNA701311	SAMN17661347	SRR13681353	MAU319	529.3	Mauritius	Raw chicken	2022	Illumina	GCA_022414795.1
PRJNA851953	SAMN29253041	SRR19787743	2010K-0348	738.4	Mauritius	Uncooked chicken	2022	Illumina	GCA_025110045.1
PRJNA230403	SAMN03145678	SRR1634586	2014EL-1195	386.8	Kenya	-	2019	Illumina	GCA_080010555.1
PRJNA230403	SAMN20456356	SRR15279128	2006773028	403.9	Kenya	Kibera	2021	Illumina	GCA_020137075.1
PRJEB634	SAMEA2053615	ERR311305	ILBSalm5484209	461.7	DR Congo	Blood	2019	Illumina	GCA_009620275.1
PRJEB634	SAMEA2053413	ERR311302	ILBSalm5484205	397.1	DR Congo	Blood	2019	Illumina	GCA_009628695.1
PRJNA219727	SAMN02352747	SRR975467	CFSAN004165	369.9	Burkina Faso	Sesame seed	2023	Illumina	GCA_025297185.1

Genome annotation and resistance gene identification

Genomes were annotated via the Comprehensive Genome Analysis service in the Bacterial and Viral Bioinformatics Resource Center (BV-BRC v3.55.17) using the RASTtk pipeline (Brettin et al., 2015). Antibiotic resistance genes were identified using the BV-BRC resistance annotation pipeline, while biocide and heavy metal resistance genes were screened against the BacMet database (Pal et al., 2014) to evaluate potential multi- and cross-resistance profiles.

Phylogenetic tree construction and SNP Calling

Single nucleotide polymorphisms (SNPs) were called from FASTQ reads using Snippy v4.6.0. Core genome SNPs were extracted via snippy-core to generate a whole-genome alignment. A maximum-likelihood phylogeny was inferred using IQ-TREE v2 under the GTR + G substitution model with 1,000 ultrafast bootstrap replicates (Li and Durbin, 2009; Garrison and Marth, 2012; Minh et al., 2020).

Pangenome Analysis

For comparative genomics, genomes were aligned against reference sequence NC_011294 and visualized using the BLAST Ring Image Generator (BRIG) (Alikhan et al., 2011). Pairwise whole-genome alignments and structural variations were further assessed in Geneious Prime using the LASTZ algorithm. Genomic similarity was quantified by calculating pairwise BLAST-based ANI values of the assembled contigs using JSpecies (Richter and Rosselló-Móra, 2009; Kim et al., 2014).

Pangenome and Average Nucleotide Identity (ANI) Analysis

For comparative genomics, genomes were aligned against reference sequence NC_011294 and visualized using the BLAST Ring Image Generator (BRIG) (Alikhan et al., 2011). Pairwise whole-genome alignments and structural variations were further assessed in Geneious Prime using the LASTZ algorithm. Genomic similarity was quantified by calculating pairwise BLAST-based ANI values of the assembled contigs using JSpecies (Richter and Rosselló-Móra, 2009; Kim et al., 2014).

Data visualization

Heatmaps representing resistance gene distribution, SNP distance matrices, Average Nucleotide Identity (ANI), and SNP-type mutation patterns were generated in RStudio (version 4.4.3) using the packages readxl, dplyr, tidyr, pheatmap, ggplot2, and RColorBrewer for data processing, transformation, and visualization.

RESULTS

The analysis examined 20 Salmonella enterica isolates from diverse African sources: Tanzania, Nigeria, South Africa, Tunisia, Malawi, Ethiopia, Uganda, Kenya, Mauritius, Democratic Republic of the Congo, and Burkina Faso. Isolates originated from human clinical specimens (blood, bone marrow, stool), food animals (poultry, pigs, cattle), and food products, reflecting broad geographic and epidemiological diversity across Africa.

Amr Gene Distribution across Antibiotic Classes

The *MdtABC-TolC* system recorded a HitScore of ~ 54 in association with novobiocin. *EmrA* and *EmrAB-TolC* were linked to nalidixic acid (HitScore 36–54), with *emrB* contributing an association against the same class. *AcrEF-TolC* showed an association with ciprofloxacin alone (~ 36), while *AcrAB-TolC* was linked to the tigecycline/rifampin/triclosan/acriflavine multi-class combination. The global regulators *marA* and *marR* each recorded HitScores of ~ 36 in association with the cefalosporin/ chloramphenicol/ tigecycline/ ampicillin multi-class group. *AcrAD-TolC* and *acrD* showed low-score associations with aminoglycosides. Contributions from *robA*, *soxS*, and *pmrG* were observed against broad-spectrum and fluoroquinolone categories respectively.

Association between AMR Genes And Chemical Disinfectants

The *emrB* gene recorded a HitScore of ~ 36 linked to the PMA/CCCP/TCS multi-biocide combination, with *emrA* showing an association with the same combination. The *acrE/envC* and *acrF/envD* components were associated with the TPP/SDC/EtBr/BAC multi-biocide group (~ 27 each), while *baeR* and *baeS* showed co-association with sodium deoxycholate. The *gesA*, *gesB*, and *gesC* genes each recorded mid-range HitScores against the methylene blue/crystal violet combination, and *MarA* and *MarR* showed associations with cyclohexane/diphenyl ether. The *cpxR* gene recorded an association with H_2O_2/BAC/chlorhexidine, while *mdtA*, *mdtB*, and *mdtC* co-occurred against sodium deoxycholate, and *emrD* showed low-score associations with both CCCCP and BAC/SDS.

Association between AMR Genes And Heavy Metal Exposure

All heavy metal efflux gene associations were recorded at a consistent HitScore of 18. The *gesA* and *gesB* genes were associated with gold (Au), while *gesC* showed a link to a gold-containing combination. The *mdtA*, *mdtB*, and *mdtC* genes were each linked to zinc (Zn) alone, and the regulatory genes *baeR* and *baeS* were both associated with the zinc/tungsten combination. The *pmrG* gene was linked to iron (Fe), *robA* to the silver/mercury/cadmium combination, and *soxS* to zinc (Zn), with an additional low-score association noted for the Zn+ multi-metal category.

Gene Associations with Functional Protein Annotations

The MAR proteins MarA and MarR recorded 36 detections each via their respective genes *marA* and *marR*. Within the RND family, the AcrEF-TolC fusion component AcrE showed gene detection in 36 strains, while AcrAB-TolC components AcrA and AcrB were each detected in 18 strains, alongside AcrD (18 detections) and the regulator AcrR (18 detections). For the MFS family, the EmrAB-OMF antiporter EmrB recorded 36 detections, with an additional 18 detections via the EmrAB-TolC system, while the fusion component EmrA and the regulator EmrR were each detected 18 times. The complete MdtABC-TolC tripartite system was uniformly represented, with MdtA, MdtB, and MdtC each recorded at 18 detections.

SNP Distance Structures and Phylogenetic Analysis

The Maximum-Likelihood phylogenetic reconstruction resolved the 20 *Salmonella enterica* isolates and the reference strain (NC_011294) into two clades and one divergent lineage, supported by bootstrap values up to 100% (Fig. 5). Clade 1 (BS = 100%) comprised 16 strains. Within Clade 1, isolate 101 (Tunisia) and ILBSalm5484205 (DRC) occupied late and early divergence positions respectively, while CFSAN031267 (Tanzania) branched at an internal node (BS = 68%). Clade 1 contained five sister pairs (BS} = 100%): 19CS0293 (Nigeria)–CFSAN072816 (Tunisia), 2014EL-1195 (Kenya)–A13198 (Malawi), CFSAN031573 (Ethiopia)–D1 (South Africa), D7 (Nigeria)–ICOPHAI16755 (Tanzania), and ILBSalm5484212–ILBSalm5484214 (both Uganda). Clade 2 (BS = 100%) consisted of 2010K-0348, MAU319 (both Mauritius), and ILBSalm5484209 (DRC). Strain Q23F2_BM (Malawi) occupied a separate, divergent branch.

Pairwise log-transformed SNP distance analysis showed two main clusters (Fig. 6). The first cluster comprised the ILBSalm isolates, Reference, Q23F2_BM, 2010K_0348, and MAU319. Pairwise log SNP distances were ~ 1–2 between 2010K_0348 and MAU319, and ~ 4–6 across the ILBSalm group. The remaining isolates clustered with log SNP distances of ~ 10–12. Isolate YA00509485 formed a separate matrix row and column with the lowest log-scaled SNP distances against all other isolates.

SNP-type pattern analysis across 33 efflux genes split the isolates into two hierarchical clusters (Fig. 7). The first cluster (ILBSalm5484212, ILBSalm5484205, 2010K_0348, MAU319, ILBSalm5484209, Q23F2_BM, and ILBSalm5484214) exhibited absent or sparse SNP patterns across the genes. The second cluster displayed synonymous and non-synonymous SNP patterns concentrated in *acrD*, *acrR*, *mdtC*, *baeS*, *emrD*, *mdtK*, *envC*, *mdtB*, and *emrA*, alongside localized non-synonymous SNPs in *pmrG*, *crp*, *soxS*, *acrA*, *marR*, *marA*, *robA*, *cpxR*, *acrB*, and *baeR*. The genes *ydhE*, *ybaH*, *tolC*, *ramA*, *mdfA*, *gesC*, *gesB*, *gesA*, *envD*, *emrR*, *bcr*, *acrE*, and *acrF* recorded zero SNP signals across all isolates.

Pangenome results

Circular whole-genome comparison of the 20 isolates against the 4,685,848 bp reference genome (NC_011294) showed continuous alignment coverage spanning most of the reference sequence across the majority of isolates (Fig. 8). Sequence absence gaps occurred at approximately 200–400 kbp, 1,600–1,800 kbp, and 2,200–2,400 kbp, with more frequent and broader gap intervals located in the outermost rings compared to the innermost rings.

Whole-genome pairwise alignment via LASTZ showed forward-strand alignment across the 4.68 Mb reference sequence, interspersed with discrete reverse-strand alignment regions clustered around 1,500,000 bp and 2,000,000–2,500,000 bp (Fig. 9). White gap regions lined up with the variable regions identified in the BRIG analysis, with alignment fragmentation coinciding with areas of dense gene annotation.

The Average Nucleotide Identity (ANI) heatmap recorded whole-genome similarity values structured into three main blocks across the collection: a baseline matrix value at approximately 98%, subsets at approximately 99%, and small diagonal clusters at approximately 100% identity (Fig. 10).

DISCUSSION

This study investigated the genomic basis of multidrug resistance (MDR) in *Salmonella enterica* isolates collected across Africa. By combining resistance gene profiling with evolutionary analysis, the research aimed to understand how resistance traits are distributed, maintained, and propagated. The findings show that resistance architecture in these isolates is shaped by three interconnected forces: regional phylogenetic relationships, co-selection driven by anthropogenic biocide and heavy metal exposure, and an intricate network of structural efflux systems under tight global regulation. By aligning whole-genome phylogeny with phenotypic markers, these data reveal a clear decoupling of the core genome from mobile, accessory resistance traits. This decoupling underscores the rapid, independent evolution of resistance within established bacterial lineages across the continent.

1. Evolutionary Architecture and Cross-Border Dissemination

The maximum-likelihood phylogenetic tree and average nucleotide identity (ANI) analyses show that the 20 investigated *S. enterica* strains did not evolve as isolated, independent entities. Instead, they cluster within well-defined ancestral lineages that transcend national borders. The observed ANI values of approximately 98% to 100% firmly establish that all isolates belong to the same species, exceeding the standard prokaryotic species boundary threshold of 95% or greater (Jain et al., 2018). Crucially, the ANI heatmap reveals distinct high-similarity clusters that pair isolates from geographically distant countries, specifically linking Nigeria with Tunisia, Kenya with Malawi, and Ethiopia with South Africa. This precise alignment between independent genomic metrics and maximum-likelihood topologies minimises the likelihood of analytical artefacts (Ondov et al., 2016) and strongly implies active cross-border transmission. In the African context, these shared lineages likely reflect regional agricultural trade, livestock movement, and food supply chains. This pattern of regional connectivity strongly aligns with continent-wide genomic epidemiology by Park et al. (2021), which demonstrated that dominant, multidrug-resistant lineages of invasive non-typhoidal *Salmonella* circulate widely across sub-Saharan borders via regional trade corridors, rather than evolving in isolated national silos. Conversely, this finding contrasts with a broad genomic survey by Ganesan et al. (2026), which identified high genetic distances among *Salmonella* isolates from various African nations and concluded there was a low likelihood of active cross-border transmission. Our discovery of distinct, high-similarity inter-country clusters suggest that while localized country-specific silos certainly exist, active regional transmission corridors are simultaneously operating across the continent. Consequently, local containment strategies are insufficient to address the continental spread of resistant *Salmonella*. Concurrently, the tight clustering of the Ugandan ILBSalm strains confirms that localised, endemic transmission loops operate in parallel with this broader regional dissemination.

Within this evolutionary landscape, the strain Q23F2_BM from Malawi emerges as a critical outlier, sitting phylogenetically apart from both primary clades. Because this strain was isolated directly from bone marrow, which signals a highly invasive and severe clinical infection, its extreme genetic uniqueness is biologically significant. This divergence suggests that Q23F2_BM represents a distinct evolutionary lineage that may possess unique virulence factors or alternative therapeutic response profiles, marking it as a critical target for future functional characterisation.

A notable finding was the unusual behaviour of isolate YA00509485, derived from a South African human stool sample. The pairwise single nucleotide polymorphism (SNP) distance analysis identified this isolate as a major outlier. It displayed anomalously low log-scaled SNP distances against all other isolates, which is inconsistent with either major cluster and reflected by its near-white row and column in the log-transformed heatmap. However, both the maximum-likelihood phylogenetic tree and ANI analysis placed it within the main isolate group, showing normal similarity levels of approximately 98% ANIb. This discordance is likely caused by the presence of a large accessory genetic element in YA00509485, such as a plasmid or prophage. The highly divergent sequence of this element may distort whole-genome SNP counts without substantially affecting core chromosomal relationships. This explanation is further supported by the BLAST Ring Image Generator (BRIG) pangenome analysis, which suggests that the variation derives primarily from accessory genes rather than the conserved chromosome.

Overall, the dataset shows high genetic diversity among the isolates. These findings highlight that whole-genome SNP distances and core genome phylogenies measure fundamentally different aspects of genomic variation. Whole-genome SNP analysis captures total genomic differences, including

mobile genetic elements, whereas core genome phylogeny mainly reflects evolutionary relationships passed through inheritance. Therefore, researchers must interpret both methods together to avoid incorrectly classifying complex strains as phylogenetic outliers (Campioni et al., 2022; Turcotte et al., 2022).

Furthermore, the comparative genomic analysis highlights a stark evolutionary dichotomy between the major isolate clades, as visualised in the SNP profiles. The near-complete absence of SNPs within the left cluster, which encompasses the Ugandan strains, the Mauritius pair, and the Democratic Republic of the Congo (DRC) isolate ILBSalm5484209, suggests a distinct evolutionary path. These lineages have either experienced minimal cumulative antimicrobial selective pressure or rely almost exclusively on horizontal gene transfer, rather than point mutations, to maintain resistance. This interpretation is directly supported by the BRIG pangenome alignments, which show highly variable accessory regions embedded within a largely conserved chromosomal backbone. Conversely, the right phylogenetic cluster exhibits extensive mutational variation, carrying both synonymous and non-synonymous mutations across an upper gene block containing critical efflux and sensor genes, including *acrD*, *acrR*, *mdtC*, *baeS*, *mdtK*, *envC*, *mdtB*, and *emrA*. The high proportion of non-synonymous substitutions in genes encoding Resistance-Nodulation-Division (RND) transporter components, such as AcrD and MdtBC, provides strong evidence of positive directional selection (Gaurav et al., 2023). These structural mutations likely alter substrate-binding pockets or efflux kinetics. This alteration directly broadens the range of expelled compounds and drives the pan-resistant phenotypes observed across the isolate collection.

2. Substrate-Specific Efflux Dynamics and Regulatory Networks

The antibiotic resistance gene heatmap shows that broad-spectrum resistance in these African isolates is mediated by a modular, structured suite of substrate-specific efflux pumps, rather than a single generalised mechanism. This multi-pump arrangement represents a classic adaptive strategy in Gram-negative pathogens, facilitating the co-occurrence of resistance to structurally unrelated drug classes within a single cell (Blair et al., 2015). A pivotal finding in this study is the unexpected dominance of the AcrEF-TolC system over the typically ubiquitous AcrAB-TolC pump as the primary mechanism associated with ciprofloxacin resistance. While researchers conventionally view AcrAB as the primary multidrug exporter in *S. enterica*, these data confirm that AcrEF can assume functional dominance under specific environmental or regulatory conditions (Alav et al., 2021). Ciprofloxacin is a frontline therapeutic agent for invasive salmonellosis in resource-limited settings, and fluoroquinolone-resistant *Salmonella* is classified as a high-priority pathogen by the World Health Organization (Chowdhury et al., 2025). Consequently, the systemic shift toward AcrEF-mediated resistance represents a significant clinical challenge. It is important to note that this dominant reliance on efflux mechanisms partially diverges from the wider scientific consensus. Global studies, such as those by Piekarska et al. (2023), maintain that high-level clinical fluoroquinolone resistance in *Salmonella* is primarily driven by target-site mutations in the Quinolone Resistance Determining Region (QRDR; *gyrA* and *parC*) or plasmid-mediated quinolone resistance (PMQR) genes. Our data, therefore, uncovers an alternative, efflux-driven evolutionary trajectory where the AcrEF-TolC system assumes primary functional dominance in these specific African lineages.

This structural diversity is balanced by highly conserved, unmutated core elements. The middle gene block, which includes the outer membrane channel *tolC*, the positive regulator *ramA*, the *gesABC* operon, and the *acrE* linker, displays a complete absence of SNPs across all 20 isolates. The absolute conservation of TolC is a biologically meaningful negative result. Because this outer membrane porin is the shared exit channel for multiple tripartite efflux complexes, its absolute stability confirms a specific evolutionary trajectory. Resistance evolution in these strains occurs via upstream regulatory tuning or inner-membrane transporter mutations rather than modifications to the structural exit portal (Jang, 2023). Interestingly, the protein product heatmap reveals an exceptionally low detection frequency for RamA. This protein typically acts as the master transcriptional activator of AcrAB-TolC in European and Asian epidemic strains (Alav et al., 2021). The near-absence of RamA in this dataset indicates that the structural pumps in these African isolates are regulated via alternative pathways, such as the Multiple Antibiotic Resistance (MAR) regulon. This illustrates that identical resistance genes can yield distinct clinical trajectories depending on the active local regulatory circuits. This independent regulatory shift is supported by foundational work from the Nikaido & Pages (2012), which established that the MAR regulon (*marA*) can orchestrate a robust downstream efflux defense completely independent of the classical *ramA* activator when bacteria respond to localized environmental stressors.

The vital role of the MAR regulon is evidenced by the universal co-detection of the *marA* activator and *marR* repressor genes, along with their respective protein products, across the entire dataset. MarA orchestrates a coordinated stress response by simultaneously upregulating downstream efflux operons and downregulating outer membrane influx porins, like OmpF, following sub-inhibitory antimicrobial exposure (Elbaiomy et al., 2025). The preservation of intact *marA* and *marR* sequences, dominated purely by synonymous mutations, suggests a highly calibrated regulatory equilibrium. Rather than representing evolutionary dead-ends, these synonymous mutations may subtly modulate translation kinetics, mRNA transcript stability, or codon usage bias. This optimises the abundance of regulatory proteins without altering their essential amino acid sequences. Furthermore, the dataset reveals a high detection frequency for the Major Facilitator Superfamily (MFS) pump EmrAB-TolC, which shows a strong statistical association against nalidixic acid. Interestingly, the inner membrane transporter *emrB* occurred at a higher frequency than its membrane fusion partner *emrA*. This asymmetric detection pattern suggests differential expression or genetic uncoupling within the tripartite operon. Such an uncoupling potentially allows excess EmrB monomers to pool in the inner membrane and enhance substrate capture prior to complex assembly (Jang, 2023). Additionally, the uniform and intact co-detection of all three structural elements of the MdtABC-TolC system in association with novobiocin confirms that this tripartite complex is functionally maintained. This maintenance avoids the total loss of efflux capacity that accompanies incomplete pump assembly.

3. Biocide Overlap and Environmental Cross-Resistance Pathways

The biocide resistance profiling shows that routine environmental hygiene practices can inadvertently preserve and amplify antibiotic resistance even in the absence of direct antibiotic exposure. This phenomenon is driven by the broad substrate profiles of RND and MFS efflux systems, which efficiently export both therapeutic drugs and chemical disinfectants (Ahmad et al., 2021). The structural components *acrA* and *acrB* exhibited strong, simultaneous associations with a diverse array of membrane-active agents, organic solvents, and antiseptics. These include phenol, acriflavine, p-xylene, cyclohexane, and triclosan. The linkage with triclosan carries significant public health implications for the African continent, where this chemical remains widely integrated into consumer soaps, hand sanitisers, and household cleaning agents. The environmental persistence of triclosan in poorly treated wastewater creates chronic,

sub-inhibitory exposure zones. These conditions systematically select for overexpressed AcrAB systems, thereby anchoring multidrug-resistant phenotypes within enteric bacterial communities (Barbosa et al., 2025).

Even more concerning is the dual role played by the AcrEF system, which shows specific associations with benzalkonium chloride (BAC), sodium deoxycholate (SDC), and sodium dodecyl sulphate (SDS). Benzalkonium chloride serves as the active baseline for quaternary ammonium compound (QAC) disinfectants, which are heavily deployed across African clinical, veterinary, and food-processing facilities. Sub-inhibitory exposure to QACs induces the transcriptional upregulation of *acrEF*, accidentally conferring cross-tolerance to fluoroquinolone antibiotics like ciprofloxacin. Because AcrEF was simultaneously identified as the dominant fluoroquinolone pump in this cohort, the widespread use of commercial QAC disinfectants establishes a direct chemical pathway that selects for clinical fluoroquinolone failures. This is particularly problematic in settings where ciprofloxacin represents a critical therapeutic backstop. This direct cross-resistance pathway is heavily corroborated by experimental findings from Mustafa et al. (2021), who demonstrated that exposure to sub-inhibitory concentrations of routine commercial disinfectants like triclosan and benzalkonium chloride directly induces the overexpression of RND-family efflux pumps, actively anchoring multidrug-resistant phenotypes in enteric pathogens even in the total absence of direct antibiotic pressure.

This cross-resistance dynamic is further reinforced by the EmrAB system, which displayed the strongest biocide associations in the entire dataset. It specifically targeted proton-motive force dissipators and hydrophobic agents like phenylmercury acetate, carbonyl cyanide 3-chlorophenylhydrazone (CCCP), and tetrachlorosalicylanilide (TCS). Because this identical pump handles nalidixic acid, its continuous induction by industrial disinfectants directly couples chemical hygiene protocols with the maintenance of quinolone resistance. This network is tied together by the *baeR* and *baeS* two-component regulatory genes, which were explicitly associated with the natural intestinal surfactant sodium deoxycholate. The BaeSR system senses envelope stress induced by bile acids, detergents, or heavy metals, and it subsequently triggers the expression of downstream multidrug pumps like MdtABC and AcrD (Gaurav et al., 2023). This integrated circuit underscores how normal physiological adaptation to the host intestinal environment inadvertently pre-arms *S. enterica* against external chemical disinfectants. However, evolutionary biology models established by researchers like Blair et al. (2015) indicate that the constitutive overexpression of massive tripartite efflux pumps typically imposes a severe metabolic fitness cost, meaning these resistant strains should theoretically be outcompeted by wild-type strains in drug-free environments. The persistence of our cohort suggests that chronic, low-level biocide pollution in the local environment effectively mitigates this fitness penalty, creating an artificial ecological niche that sustains these costly mechanisms.

4. Agricultural and Industrial Metal Co-Selection Pressures

The metal resistance profiles provide clear evidence that heavy metal pollution in industrial and agricultural settings acts as an alternative selective force. This pressure sustains antibiotic resistance genes (ARGs) independently of clinical antibiotic use. A striking example of this is the exclusive, unmutated conservation of the *gesA*, *gesB*, and *gesC* genes in absolute association with gold (Au). The global distribution of the *ges* operon within clinical *Salmonella* genomes points to an ancient, conserved detoxification system (De Lorenzi et al., 2025). In this cohort, the preservation of the *ges* complex correlates strongly with regional economics. Gold mining is a dominant industrial driver across several of the source countries, including South Africa, Tanzania, and the Democratic Republic of the Congo. Environmental runoff from these mining operations exposes local ecosystems to elevated gold and heavy metal concentrations. This provides the sustained selective pressure required to maintain the *ges* operon. Because these identical *gesABC* genes were simultaneously mapped to phenicol and carbapenem resistance markers, environmental gold contamination directly co-selects for resistance against last-resort human antibiotics.

A parallel co-selection matrix is visible in the agricultural sector, where *mdtABC* was associated with zinc (Zn) and *baeSR* was linked to a combined zinc-tungsten profile. In many African countries, zinc oxide is routinely added to livestock and poultry feed at sub-therapeutic doses to stimulate growth and manage post-weaning enteric infections. Chronic exposure to these sub-inhibitory zinc concentrations inside the animal gut environment triggers the BaeSR envelope stress response, upregulating the MdtABC efflux complex (Bazzi et al., 2020). Because several isolates in this collection were recovered from poultry production chains in Nigeria, South Africa, and Mauritius, these zinc-associated resistance profiles reflect the molecular footprint of commercial animal husbandry practices. This selective loop is reinforced by the presence of the *mdtK* gene. This Multidrug and Toxic Compound Extrusion (MATE) family transporter uses proton or sodium gradients, rather than ATP, to drive drug efflux, adding energetic versatility to the cellular resistance profile.

Finally, the detection of the transcriptional regulators *robA*, associated with silver, mercury, and cadmium, alongside *soxS*, associated with zinc, confirms that these isolates possess intact oxidative and metal-stress sensing networks. These networks are capable of driving generalised efflux responses upon heavy metal exposure. This is supported by the presence of *pmrG*, a gene downstream of the PmrAB two-component system. This gene modifies the lipopolysaccharide structure of the bacterial outer membrane in response to ambient iron concentrations, simultaneously preventing the binding of toxic metal ions and cationic antimicrobial peptides (Gunn, 2008). Crucially, all gene-metal associations in this panel were restricted to a uniform frequency of 18 isolates, rather than being universally distributed across the entire collection. This discrete, bounded distribution confirms that these metal-resistance modules reside within the accessory pangenome. They are likely carried on mobile genetic elements, such as transposable units or plasmids, shared within specific regional sub-lineages. This clear decoupling of core genomic phylogeny from accessory resistance content proves that horizontal gene transfer can rapidly reshape the resistance landscape of *S. enterica* independently of slow vertical evolution. This process is actively catalysed by heavy metal and biocide co-selection pressures in mining and farming environments. Ultimately, this co-selection paradigm is a rising reality across the continent. A recent comparative analysis by Gillieatt and Coleman (2024) confirms that *Salmonella* strains harboring heavy metal resistance genes on mobile elements yield significantly broader antimicrobial resistance profiles. Furthermore, environmental genomic surveillance by Duze et al. (2026) recently isolated highly divergent, multi-drug resistant *S. enterica* strains directly from contaminated urban water systems in South Africa. This strongly validates our conclusion that heavy metal runoff acts as a primary, non-clinical catalyst anchoring critical resistance traits within the accessory pangenome of African lineages.

CONCLUSION

This study provides critical genomic and phylogenetic insights into the distribution and evolution of multidrug resistance (MDR) in *Salmonella enterica* isolates from diverse African sources. By integrating whole-genome analysis, resistance gene profiling, and phylogenetic reconstruction, this research shows that antimicrobial resistance in *S. enterica* is not randomly distributed. Instead, it is actively shaped by an intersection of evolutionary lineage, anthropogenic co-selection pressures, and intricate regulatory networks. The findings reveal widespread multidrug resistance across the analysed isolates, with resistance determinants spanning multiple clinically vital antibiotic classes. These classes include beta-lactams, fluoroquinolones, tetracyclines, phenicols, and carbapenems. The co-occurrence of resistance to structurally unrelated antibiotics highlights the importance of shared resistance mechanisms in driving broad-spectrum resistance. Modular multidrug efflux systems and mobile genetic elements are particularly significant in this regard. These patterns pose a severe threat to current treatment options across the continent and reinforce growing concerns surrounding the longevity of last-line antibiotics.

Importantly, this study shows that non-antibiotic antibacterials, specifically biocides and heavy metals, play a significant role in the maintenance and amplification of antimicrobial resistance. Strong associations exist between resistance genes and exposure to disinfectants, detergents, solvents, and heavy metals, including gold, zinc, silver, mercury, and cadmium. These associations indicate active co-selection processes. This underscores the role of environmental, industrial, and agricultural pollutants in sustaining resistance networks even in the absence of direct antibiotic pressure. Efflux pumps belonging to the RND, MFS, and MATE families emerged as the central structural drivers of this cross-resistance. Tripartite complexes such as AcrAB-TolC, AcrEF-TolC, and Mdt transporters operate under the global coordination of the MarA/MarR regulon and stress-response pathways like SoxS and Rob. This arrangement underscores that resistance in *S. enterica* is largely a systems-level, regulatory phenomenon rather than one dependent on isolated resistance genes. Notably, the near-absence of RamA regulation indicates a unique regional reliance on alternative regulatory circuits to maintain these structural pumps.

Phylogenetic and ANI analyses further revealed that while core bacterial lineages are closely linked to cross-border dissemination, the distribution of resistance genes is heavily decoupled from vertical ancestry. Highly similar core genomes frequently display divergent resistance profiles. This divergence confirms that horizontal gene transfer via the accessory pangenome is rapidly reshaping the epidemiologic landscape of *S. enterica* independently of slow phylogenetic drift. This horizontal transfer is further accelerated by localised environmental and agricultural pressures. Ultimately, this study highlights that multidrug resistance in African *S. enterica* is a complex byproduct of evolutionary history, regulatory adaptation, and environmental co-selection. These findings reinforce the critical need to address both antibiotic and non-antibiotic drivers of resistance within a unified One Health framework.

RECOMMENDATIONS

Based on the findings of this study, the following recommendations are proposed:

1. Strengthen Regional Genomic Surveillance Programmes

Routine whole-genome sequencing (WGS) of Salmonella enterica isolates should be systematically expanded across clinical, agricultural, and environmental sectors in sub-Saharan Africa. Integrating high-resolution phylogenetic and ANI mapping into centralized surveillance systems will improve cross-border outbreak tracking, identify highly invasive lineages (such as bone-marrow-derived strains), and enable early detection of emerging MDR clones.

2. Regulate Non-Antibiotic Antibacterial Targets

Aversive policies governing the environmental and industrial discharge of heavy metals and biocides must be integrated into national AMR mitigation strategies. Specific attention should be paid to regulating sub-therapeutic zinc oxide additives in regional poultry husbandry and managing heavy metal runoff (particularly gold, silver, and mercury) in active industrial mining zones, which actively anchor last-resort antibiotic resistance genes in the ecosystem.

3. Implement Sector-Specific One Health Monitoring

AMR control strategies must move beyond clinical facilities to sample high-intensity co-selection environments. This includes coordinated, continuous surveillance of the accessory pangenome within wastewater systems, animal processing plants, and consumer hygiene products (e.g., triclosan-containing formulations) to break the cross-resistance loop between environmental biocide exposure and clinical fluoroquinolone failure.

4. Reinforce Antimicrobial Stewardship

Stewardship programmes must be aggressively enforced in both human medicine and veterinary practices to reduce unnecessary broad-spectrum antimicrobial exposure. Restricting the unmanaged use of frontline fluoroquinolones (such as ciprofloxacin) and protecting last-line carbapenems is vital to slow the evolutionary drive favoring highly adaptive regulatory efflux systems.

REFERENCES

1. Ahmad I, Malak HA, Abulreesh HH (2021) Environmental antimicrobial resistance and its drivers: a potential threat to public health. J global Antimicrob Resist 27:101–111
2. Alav I, Bavro VN, Blair JM (2021) Interchangeability of periplasmic adaptor proteins AcrA and AcrE in forming functional efflux pumps with AcrD in Salmonella enterica serovar Typhimurium. J Antimicrob Chemother 76(10):2558–2564
3. Alikhan NF, Petty NK, Zakour B, N. L., Beatson SA (2011) BLAST Ring Image Generator (BRIG): simple prokaryote genome comparisons. BMC Genomics 12(1):402
4. Allard JB, Kumar S (2025) MEGA-GPT: artificial intelligence guidance and building analytical protocols using MEGA software. Mol Biol Evol 42(6):msaf101

5. Barbosa FB, Takeda BR, Vicentini GG, Gandolfi G, Rocha VG, Franco LS, Cunha MP, Knöbl T (2025) Impact of Exposure to Disinfectants on Presence of Efflux Pump Genes and Antibiotic Resistance Profiles in Escherichia coli Isolates. Microorganisms 13(12):2700. https://doi.org/10.3390/microorganisms13122700
6. Bazzi W, Abou Fayad AG, Nasser A, Haraoui LP, Dewachi O, Abou-Sitta G, Nguyen VK, Abara A, Karah N, Landecker H, Knapp C, McEvoy MM, Zaman MH, Higgins PG, Matar GM (2020) Heavy Metal Toxicity in Armed Conflicts Potentiates AMR in A. Baumannii by Selecting for Antibiotic and Heavy Metal Co-resistance Mechanisms. Front Microbiol 11:483936. https://doi.org/10.3389/fmicb.2020.00068
7. Blair JM, Webber MA, Baylay AJ, Ogbolu DO, Piddock LJ (2015) Molecular mechanisms of antibiotic resistance. Nat Rev Microbiol 13(1):42–51
8. Campioni F, Vilela FP, Cao G, Kastanis G, Costa RG, Tiba-Casas MR, Yin L, Allard M, Falcão JP (2022) Whole genome sequencing analyses revealed that Salmonella enterica serovar Dublin strains from Brazil belonged to two predominant clades. Sci Rep 12(1):10555. https://doi.org/10.1038/s41598-022-14492-4
9. Chowdhury G, Bhattacharya S, Goel G, Chatterji SN, Kitahara K, Ohno A, Mukhopadhyay AK (2025) Phenotypic and potential virulence features of salmonella enterica serotypes from cancer patients in kolkata, india. BMC Infect Dis 25(1). https://doi.org/10.1186/s12879-025-11679-8
10. De Lorenzi G, Gherpelli Y, Scaltriti E, Bracchi C, Vinci M, Bolzoni L, Luppi A (2025) Antimicrobial resistance in Salmonella enterica serovar Choleraesuis isolated from pigs in northern Italy. Res Vet Sci 193:105773
11. Di Maso AM, Ruiz C (2024) Physiological Effects of TolC-Dependent Multidrug Efflux Pumps in Escherichia coli: Impact on Motility and Growth Under Stress Conditions. MicrobiologyOpen 13(6):e70006. https://doi.org/10.1002/mbo3.70006
12. Duze ST, Marimani M, Patel M (2026) Draft genome of extended-spectrum β-lactamase-producing multidrug-resistant *Salmonella enterica* serovar Brandearup strain DE0603 from an urban river in South Africa. Microbiol resource announcements 15(3):e0095725. https://doi.org/10.1128/mra.00957-25
13. Elbaiomy RG, El-Sappah AH, Guo R, Luo X, Deng S, Du M, Zhang Z (2025) Antibiotic Resistance: A Genetic and Physiological Perspective. MedComm, 6(11), e70447
14. Endale H, Mathewos M, Abdeta D (2023) Potential causes of spread of antimicrobial resistance and preventive measures in one health perspective-a review. Infect drug Resist, 7515–7545
15. Ganesan B, Azuma H, Baker RC, Ferreira JP, LeJeune JT (2026) Impact of databases on genomic survey of Salmonella antimicrobial resistance and virulence factor functional genes across the African continent. https://doi.org/10.64898/2026.01.14.699574
16. Garrison E, Marth G (2012) Haplotype-based variant detection from short-read sequencing. *ArXiv*. https://arxiv.org/abs/1207.3907
17. Gaurav A, Bakht P, Saini M, Pandey S, Pathania R (2023) Role of bacterial efflux pumps in antibiotic resistance, virulence, and strategies to discover novel efflux pump inhibitors. Microbiology 169(5):001333
18. Gillieatt BF, Coleman NV (2024) Unravelling the mechanisms of antibiotic and heavy metal resistance co-selection in environmental bacteria. FEMS Microbiol Rev 48(4):fuae017. https://doi.org/10.1093/femsre/fuae017
19. Gunn JS (2008) The Salmonella PmrAB regulon: lipopolysaccharide modifications, antimicrobial peptide resistance and more. Trends Microbiol 16(6):284–290
20. Han J, Aljahdali N, Zhao S, Tang H, Harbottle H, Hoffmann M, Frye JG, Foley SL (2024) Infection biology of Salmonella enterica. EcoSal Plus 12(1). https://doi.org/10.1128/ecosalplus.esp-0001-2023. eesp-0001-2023
21. Jang S (2023) AcrAB–TolC, a major efflux pump in Gram negative bacteria: Toward understanding its operation mechanism. BMB Rep 56(6):326. https://doi.org/10.5483/BMBRep.2023-0070
22. Li H, Durbin R (2009) Fast and accurate short read alignment with Burrows–Wheeler transform. Bioinformatics 25(14):1754–1760
23. Minh BQ, Schmidt HA, Chernomor O, Schrempf D, Woodhams MD, Von Haeseler A, Lanfear R (2020) IQ-TREE 2: new models and efficient methods for phylogenetic inference in the genomic era. Mol Biol Evol 37(5):1530–1534
24. Mkangara M (2023) Prevention and control of human Salmonella enterica infections: An implication in food safety. Int J Food Sci 2023(1):8899596. https://doi.org/10.1155/2023/8899596
25. Mustafa GR, Zhao K, He X, Chen S, Liu S, Mustafa A, He L, Yang Y, Yu X, Penttinen P, Ao X, Liu A, Shabbir MZ, Xu X, Zou L (2021) Heavy Metal Resistance in Salmonella Typhimurium and Its Association With Disinfectant and Antibiotic Resistance. Front Microbiol 12:702725. https://doi.org/10.3389/fmicb.2021.702725
26. Nikaido H, Pagès JM (2012) Broad-specificity efflux pumps and their role in multidrug resistance of Gram-negative bacteria. FEMS Microbiol Rev 36(2):340–363. https://doi.org/10.1111/j.1574-6976.2011.00290.x
27. Nnaji ND, Anyanwu CU, Miri T, Onyeaka H (2024) Mechanisms of Heavy Metal Tolerance in Bacteria: A Review. Sustainability 16(24):11124. https://doi.org/10.3390/su162411124
28. Parada J, Galas M, Faccone D, Tamiozzo P, Carranza A (2022) Antibiotic resistance and associated resistance determinants in different Salmonella enterica serovars isolated from pigs in Argentina. Veterinary World 15(5):1215. https://doi.org/10.14202/vetworld.2022.1215-1220
29. Park SE, Pham DT, Pak GD, Panzner U, Maria Cruz Espinoza L, von Kalckreuth V, Im J, Mogeni OD, Schütt-Gerowitt H, Crump JA, Breiman RF, Adu-Sarkodie Y, Owusu-Dabo E, Rakotozandrindrainy R, Soura B, Aseffa A, Gasmelseed A, Sooka N, Keddy A, May KH, Marks J, F (2021) The genomic epidemiology of multi-drug resistant invasive non-typhoidal *Salmonella* in selected sub-Saharan African countries. BMJ global health 6(8):e005659. https://doi.org/10.1136/bmjgh-2021-005659
30. Piekarska K, Wołkowicz T, Zacharczuk K, Stepuch A, Gierczyński R (2023) The Mechanisms Involved in the Fluoroquinolone Resistance of *Salmonella enterica* Strains Isolated from Humans in Poland, 2018–2019: The Prediction of Antimicrobial Genes by In Silico Whole-Genome Sequencing. Pathogens

(Basel Switzerland) 12(2):193. https://doi.org/10.3390/pathogens12020193

31. Putman M, Konings WN (2000) Molecular Properties of Bacterial Multidrug Transporters. Microbiol Mol Biol Rev 64(4):672. https://doi.org/10.1128/mmbr.64.4.672-693.2000
32. Sambaza SS, Naicker N (2023) Contribution of wastewater to antimicrobial resistance: A review article. J Global Antimicrob Resist 34:23–29. https://doi.org/10.1016/j.jgar.2023.05.010
33. Sánchez-Corona CG, Gonzalez-Avila LU, Hernández-Cortez C, Rojas-Vargas J, Castro-Escarpulli G, Castelán-Sánchez HG (2025) Impact of Heavy Metal and Resistance Genes on Antimicrobial Resistance: Ecological and Public Health Implications. Genes 16(6):625. https://doi.org/10.3390/genes16060625
34. sDe Lorenzi G, Gherpelli Y, Scaltriti E, Bracchi C, Vinci M, Bolzoni L, Pongolini S, Bonilauri P, Bassi P, Barbieri I, Pupillo G, Rosignoli C, Rugna G, Fiorentini L, Luppi A (2025) Antimicrobial resistance in Salmonella enterica serovar Choleraesuis isolated from pigs in northern Italy. Res Vet Sci 193:105773. https://doi.org/10.1016/j.rvsc.2025.105773
35. Seemann T (2015) snippy: fast bacterial variant calling from NGS reads.(version 4.6. 0)
36. Sheu CC, Chang YT, Lin SY, Chen YH, Hsueh PR (2019) Infections Caused by Carbapenem-Resistant Enterobacteriaceae: An Update on Therapeutic Options. Front Microbiol 10:435078. https://doi.org/10.3389/fmicb.2019.00080
37. Souza SS, Turcotte MR, Li J, Zhang X, Wolfe KL, Gao F, Benton CS, Andam CP (2022) Population analysis of heavy metal and biocide resistance genes in Salmonella enterica from human clinical cases in New Hampshire, United States. Front Microbiol 13:983083. https://doi.org/10.3389/fmicb.2022.983083
38. Thota SS, Chubiz LM (2019) Multidrug Resistance Regulators MarA, SoxS, Rob, and RamA Repress Flagellar Gene Expression and Motility in Salmonella enterica Serovar Typhimurium. J Bacteriol 201(23):e00385–e00319. https://doi.org/10.1128/JB.00385-19
39. Turcotte MR, Commins N, Li J, Zhang X, Wolfe KL, Gao F, Andam CP (2022) Genome characteristics of clinical Salmonella enterica population from a state public health laboratory, New Hampshire. BMC Genomics 23(1):2017–2020. https://doi.org/10.1186/s12864-022-08769-1
40. Turcotte MR, Smith JT, Li J, Zhang X, Wolfe KL, Gao F, Andam CP (2022) Genome characteristics of clinical Salmonella enterica population from a state public health laboratory, New Hampshire, USA, 2017–2020. BMC genomics, 23(1), 537
41. Wan J, Gao X, Liu F (2024) Regulatory role of the Cpx ESR in bacterial behaviours. Virulence 15(1):2404951. https://doi.org/10.1080/21505594.2024.2404951
42. Wand ME, Sutton JM (2022) Efflux-mediated tolerance to cationic biocides, a cause for concern? Microbiology 168(11):001263

Figures

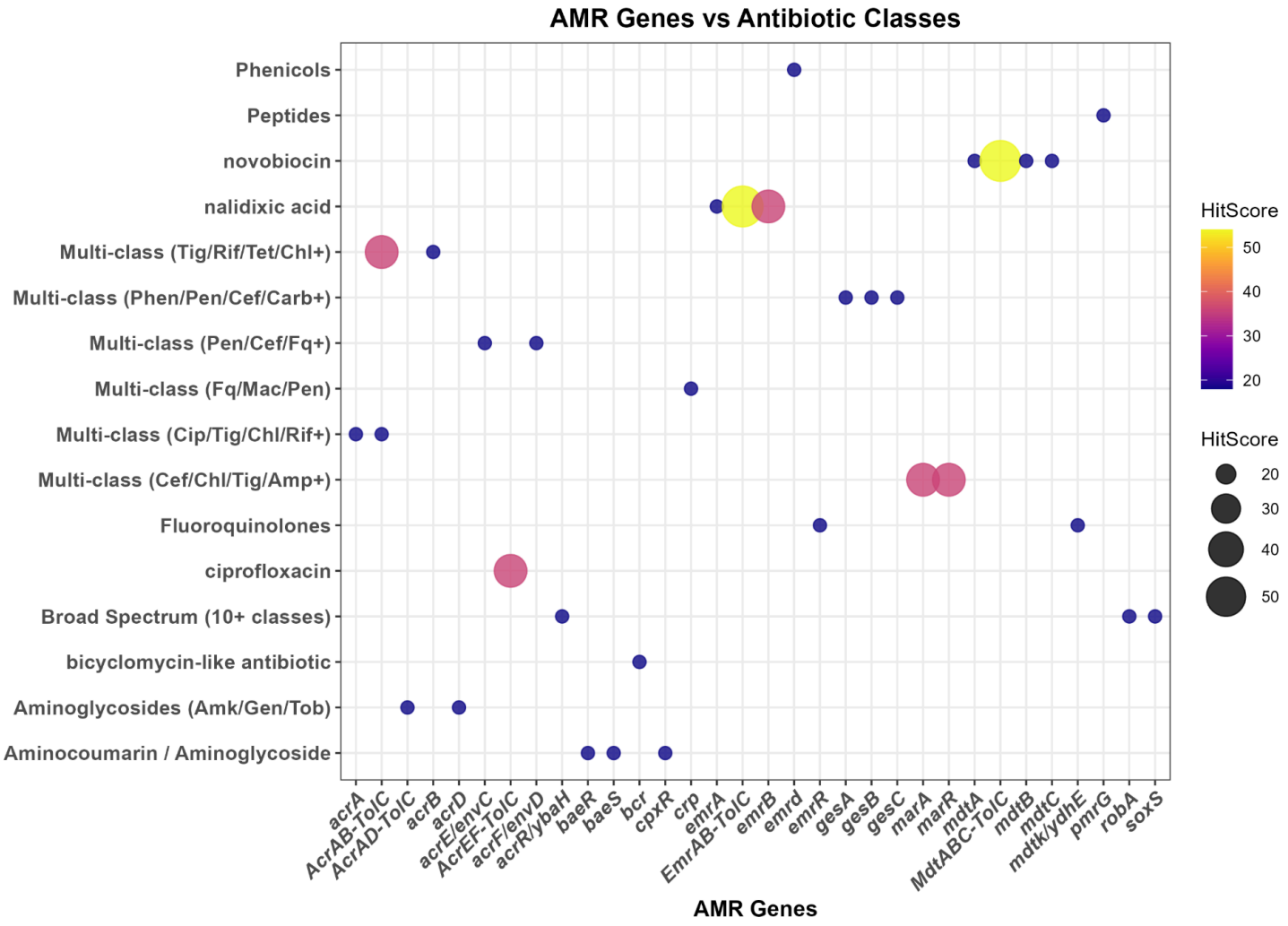


Figure 1

AMR gene associations with antibiotic resistance classes in African Salmonella enterica isolates. Bubble plot displaying efflux pump-associated AMR genes and their associations with antibiotic/drug classes detected across 20 isolates via BV-BRC annotation. Each bubble represents a gene–antibiotic class pair; bubble size and colour intensity both reflect HitScore (cumulative detection frequency), ranging from 18 (small, dark blue) to 54 (large, yellow). Antibiotic classes are ordered on the y-axis and AMR genes on the x-axis. Only gene–class pairs with at least one detection are shown.

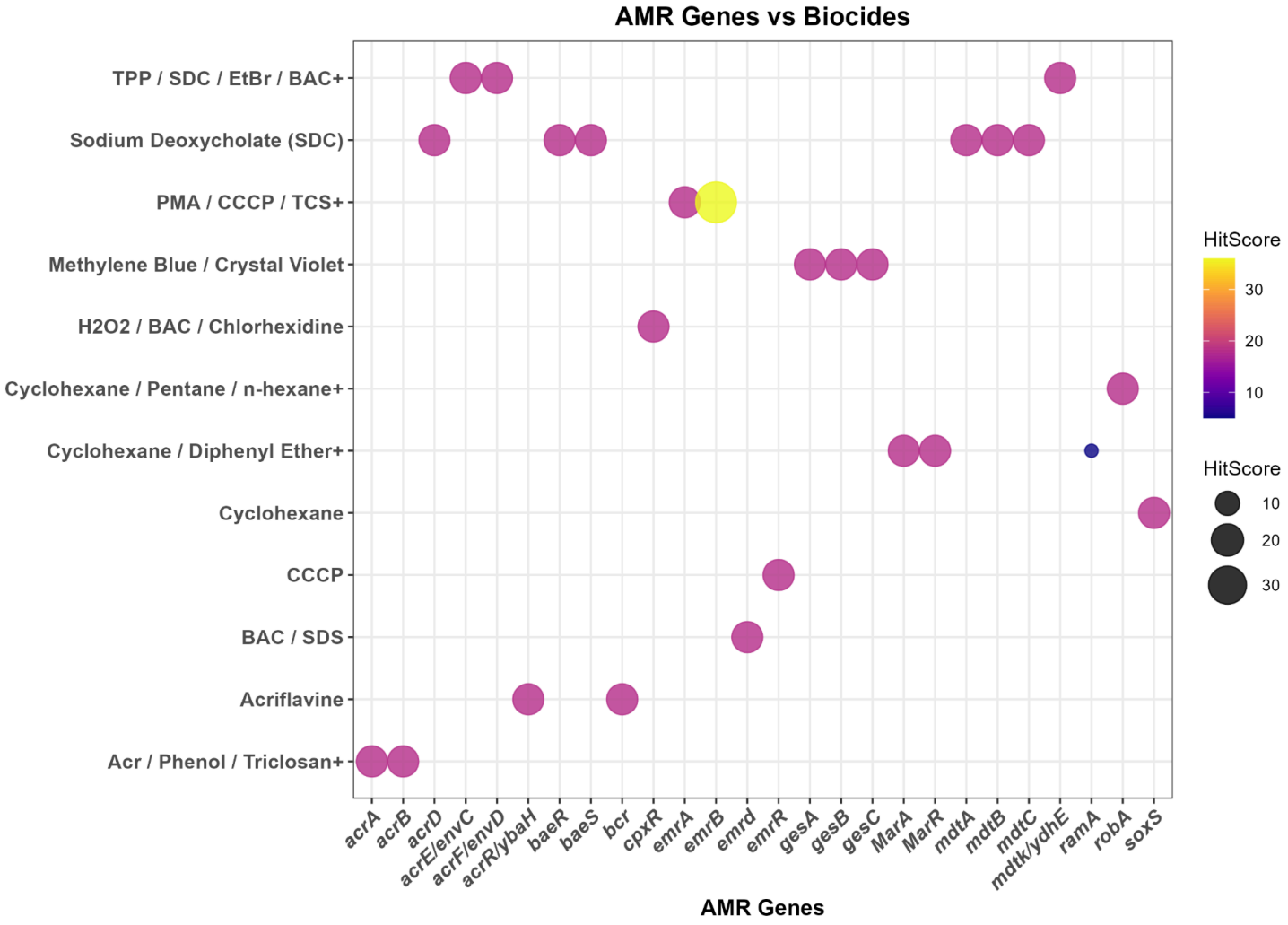


Figure 2

AMR gene associations with biocide and disinfectant resistance in African Salmonella enterica isolates. Bubble plot showing efflux pump-associated AMR genes and their associations with biocide/disinfectant combinations detected across 20 isolates via BV-BRC annotation. Each bubble represents a gene–biocide pair; bubble size and colour intensity both reflect HitScore (cumulative detection frequency), ranging from low (small, dark blue) to high (large, yellow). Biocide combinations are ordered on the y-axis and AMR genes on the x-axis. Only gene–biocide pairs with at least one detection are shown.

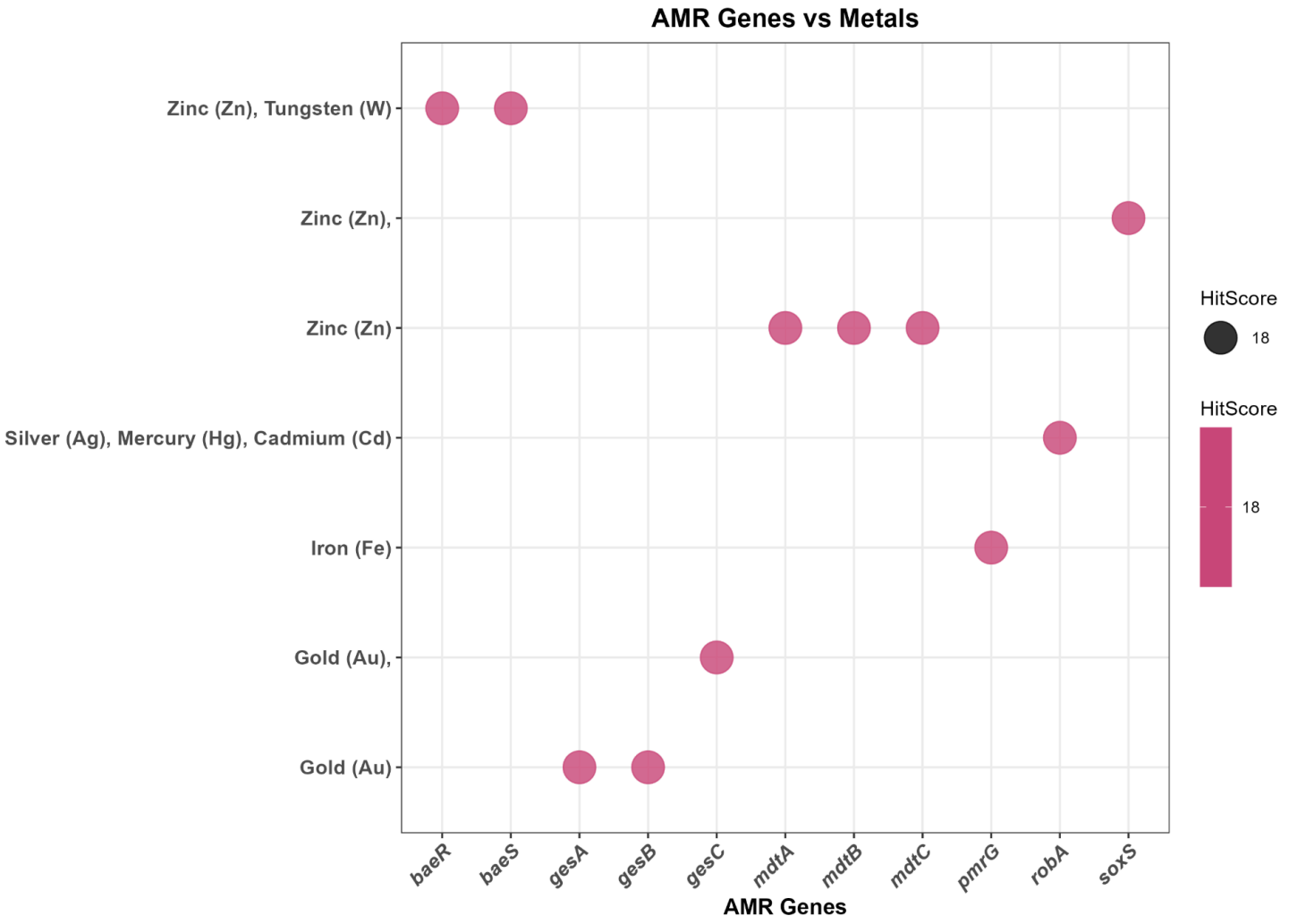


Figure 3

AMR gene associations with metal compound resistance in African Salmonella enterica isolates. Bubble plot illustrating associations between efflux pump-associated AMR genes and metal or metal combinations detected across 20 isolates via BV-BRC annotation. Each bubble represents a gene–metal pair; bubble size reflects detection frequency (HitScore). All associations in this dataset were recorded at a uniform HitScore of 18. AMR genes are ordered on the x-axis and metal combinations on the y-axis. Only gene–metal pairs with at least one detection are shown. Metal abbreviations: Au, gold; Fe, iron; Ag, silver; Hg, mercury; Cd, cadmium; Zn, zinc; W, tungsten.

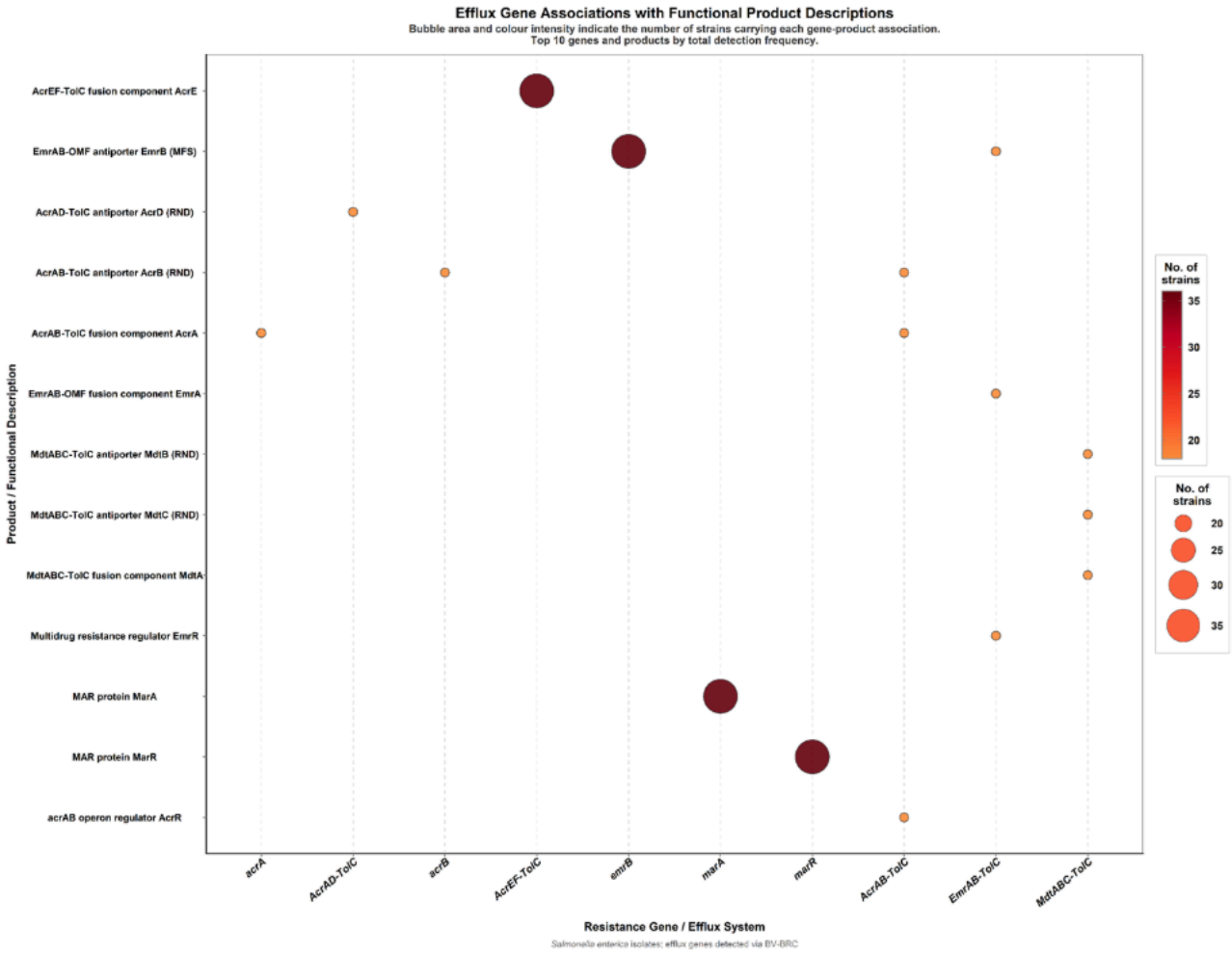


Figure 4

AMR gene associations with functional protein descriptions in African Salmonella enterica isolates. Bubble plot displaying the top 10 resistance genes mapped against their annotated functional protein product descriptions, detected across 20 isolates via BV-BRC annotation. Each bubble represents a gene–product pair; bubble size and colour intensity both reflect the number of strains carrying that association, ranging from 18 (small, light orange) to 36 (large, dark red). Genes are ordered on the x-axis and functional product descriptions on the y-axis by total detection frequency. Only gene–product pairs with at least one detection are shown.

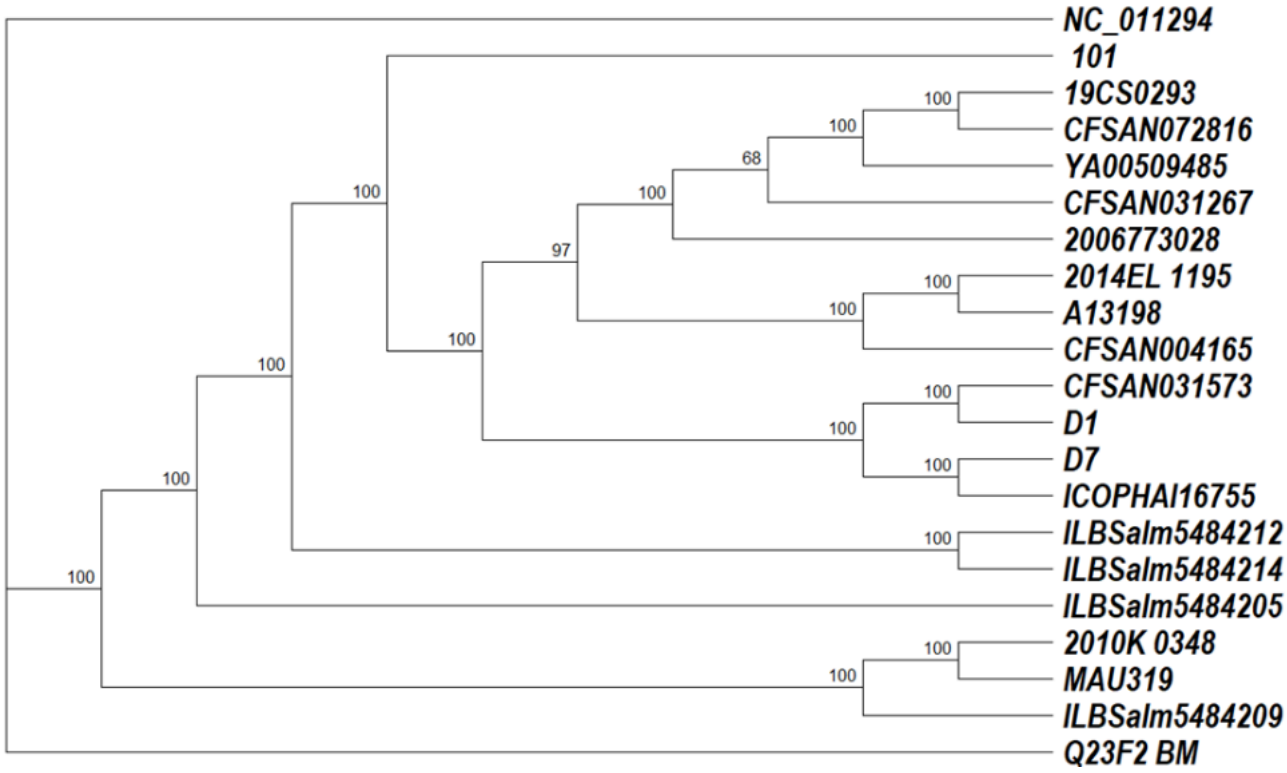


Figure 5

Maximum likelihood phylogenetic tree of Salmonella enterica African isolates and reference genome.

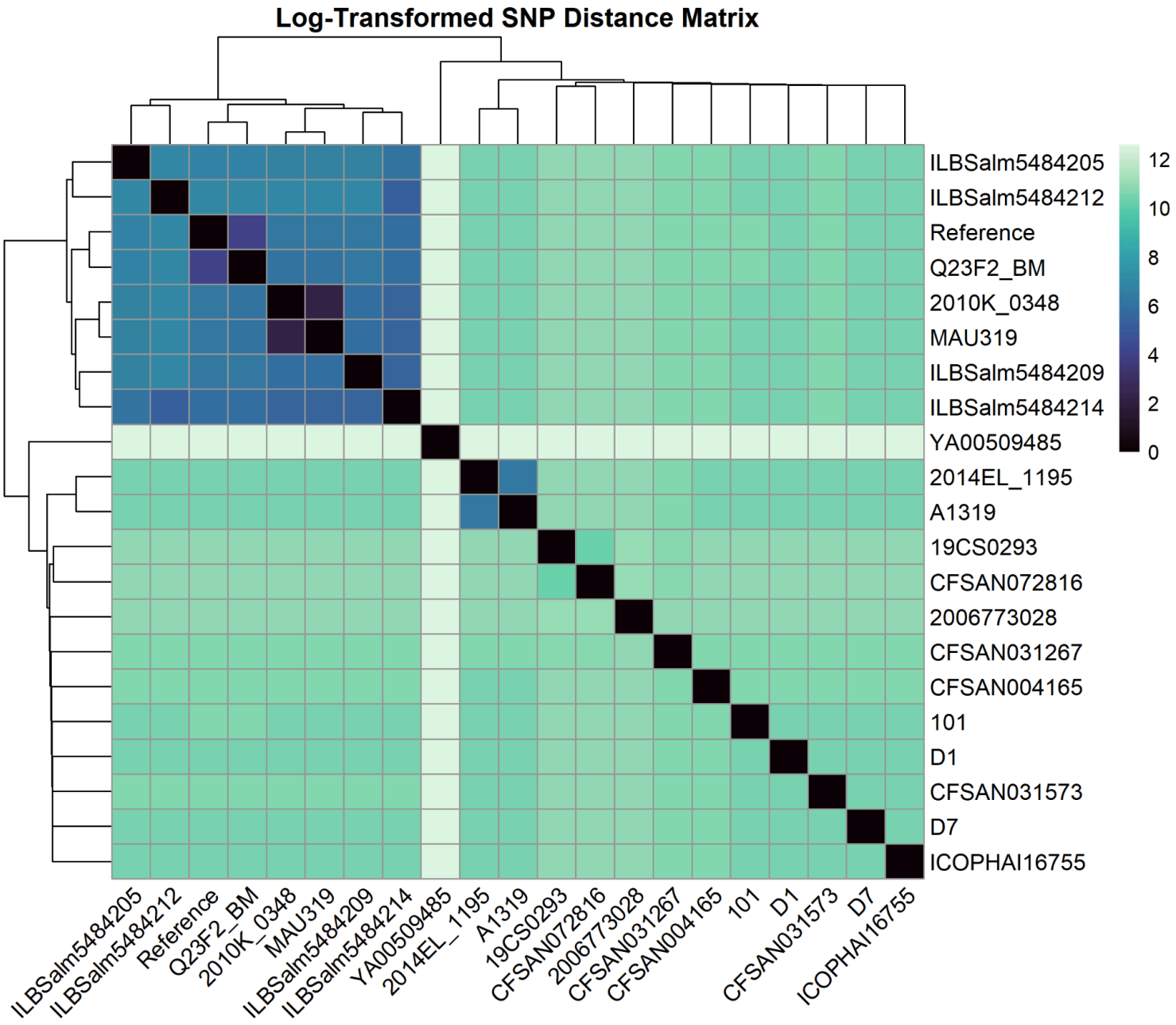


Figure 6

Pairwise SNP distance matrix of Salmonella enterica African isolates and reference genome. The heatmap displays log-transformed pairwise SNP distances between 20 Salmonella enterica African isolates and the reference genome NC_011294 (labelled "Reference"), calculated from whole-genome SNP calling using Snippy. Each cell represents the log-scaled SNP count between two isolates; darker cells (black/purple) indicate lower SNP distances (closer genomic relatedness) and lighter cells (teal/cyan) indicate greater divergence. The diagonal represents self-comparisons (SNP distance = 0). The near-white row and column corresponding to YA00509485 reflects anomalously low log-scaled distances against all other isolates, producing a visually distinct pattern inconsistent with either major cluster, likely driven by accessory genomic content rather than true chromosomal divergence. Hierarchical clustering dendrograms are shown along both axis.

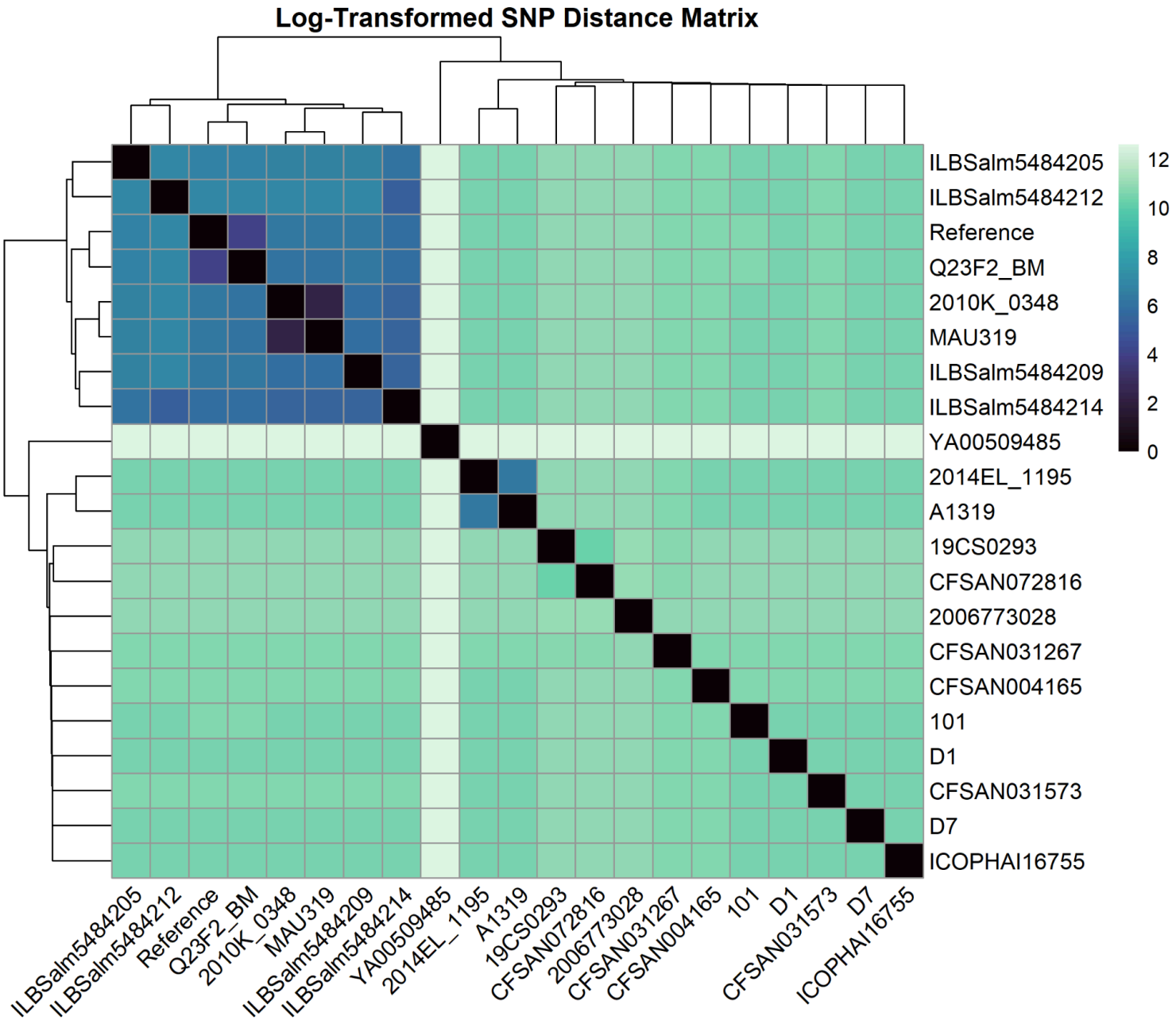


Figure 6

Pairwise SNP distance matrix of Salmonella enterica African isolates and reference genome. The heatmap displays log-transformed pairwise SNP distances between 20 Salmonella enterica African isolates and the reference genome NC_011294 (labelled "Reference"), calculated from whole-genome SNP calling using Snippy. Each cell represents the log-scaled SNP count between two isolates; darker cells (black/purple) indicate lower SNP distances (closer genomic relatedness) and lighter cells (teal/cyan) indicate greater divergence. The diagonal represents self-comparisons (SNP distance = 0). The near-white row and column corresponding to YA00509485 reflects anomalously low log-scaled distances against all other isolates, producing a visually distinct pattern inconsistent with either major cluster, likely driven by accessory genomic content rather than true chromosomal divergence. Hierarchical clustering dendrograms are shown along both axis.

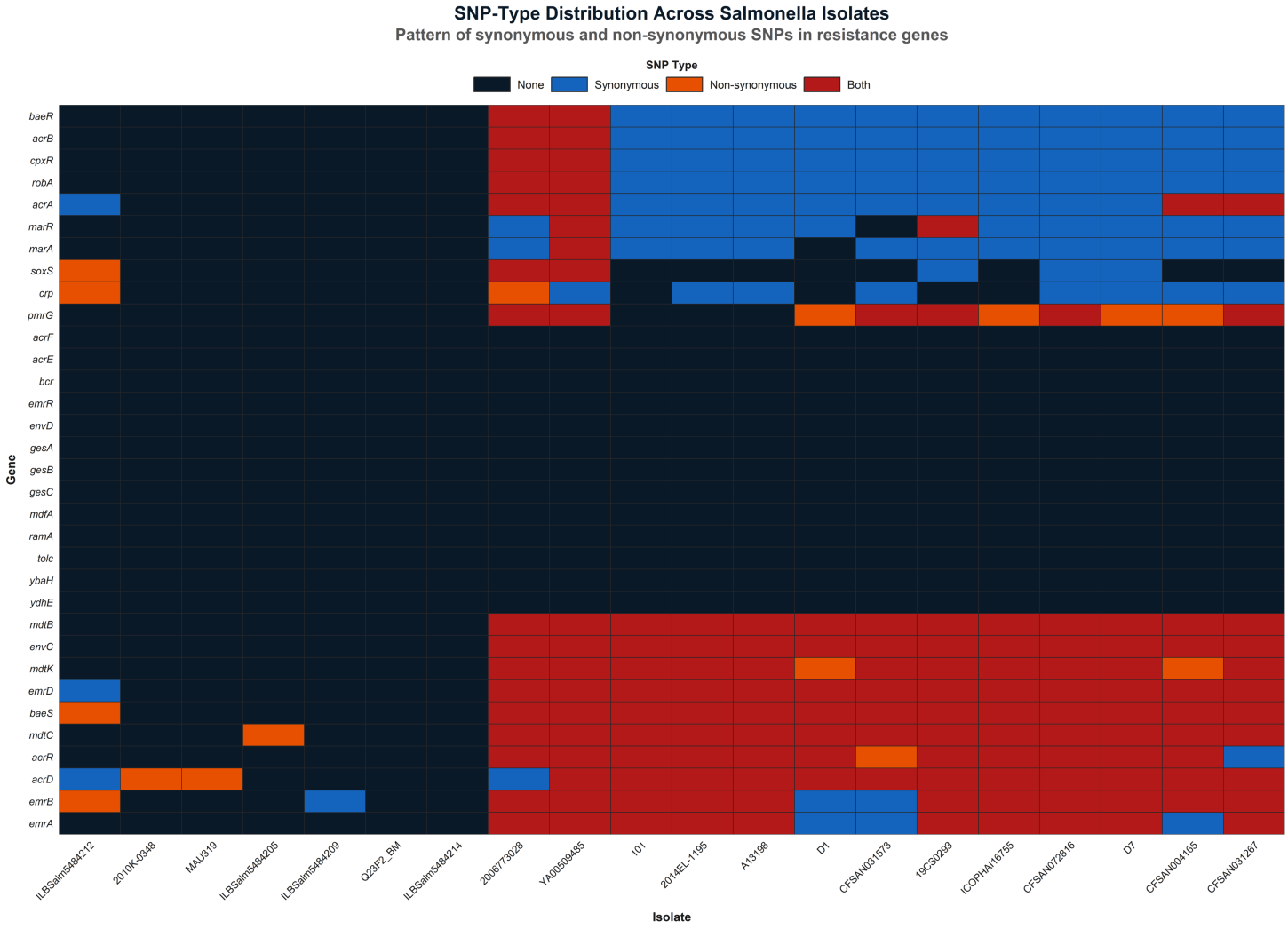


Figure 7

Heatmap of SNP-type patterns across efflux resistance genes in Salmonella enterica African isolates. The heatmap displays the SNP mutation type detected in each efflux-associated gene (Y-axis) across 20 Salmonella enterica African isolates (X-axis), as identified by whole-genome SNP calling using Snippy against the reference genome NC_011294. Cell colour represents the SNP type category: dark navy = no SNP detected (0); blue = synonymous SNP only (1); orange = non-synonymous SNP only (2); red = both synonymous and non-synonymous SNPs detected (3). Isolates and genes are hierarchically clustered using Ward's D2 linkage method based on SNP pattern similarity, with clustering applied along both axes.

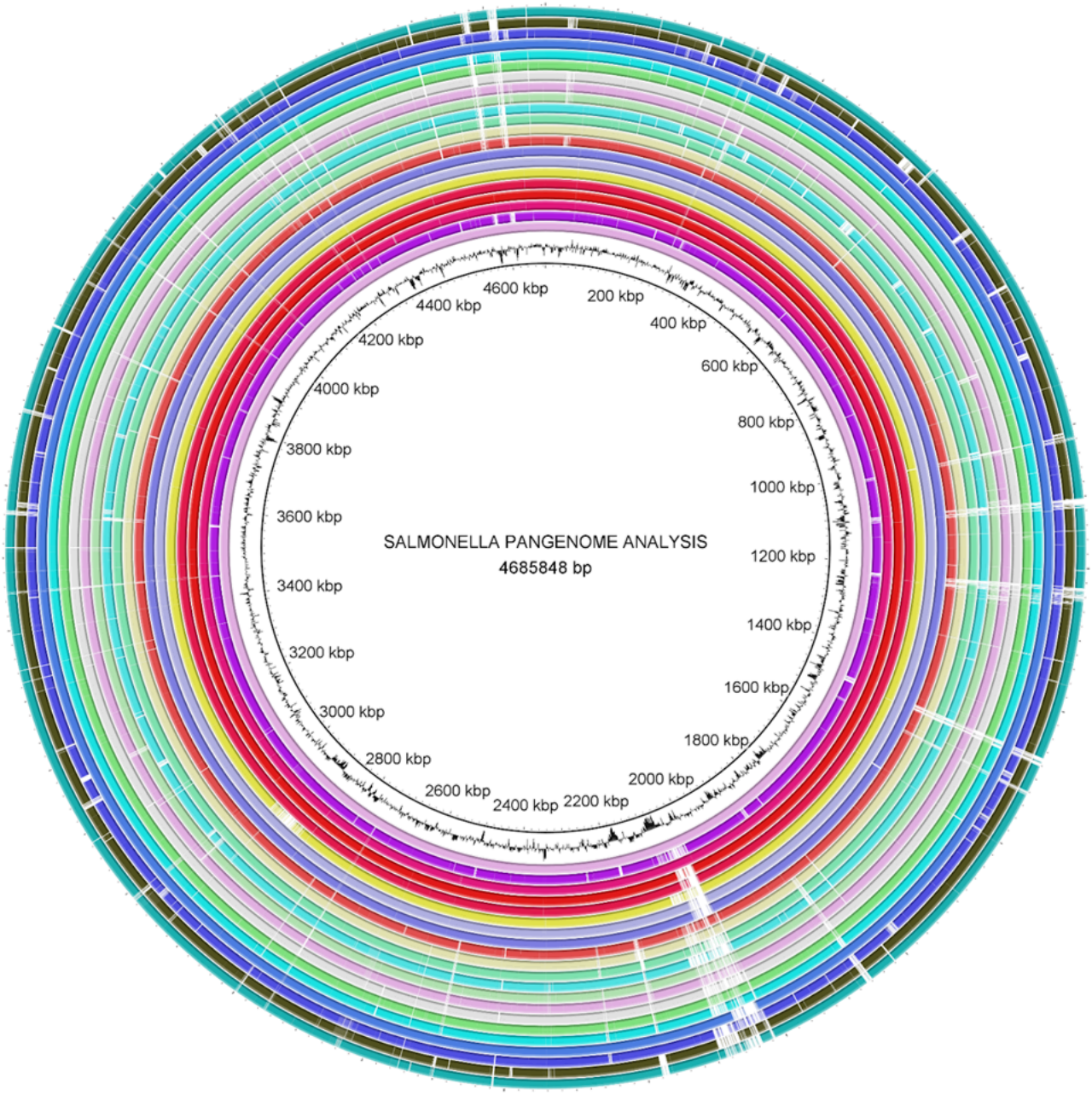


Figure 8

BRIG circular genome comparison of Salmonella enterica African isolates against the reference genome NC_011294. The circular map was generated using the Blast Ring Image Generator (BRIG) and displays whole-genome sequence comparisons between 20 Salmonella enterica African isolates and the reference genome NC_011294 (Salmonella enterica subsp. enterica serovar Typhimurium str. LT2; 4,685,848 bp). Each concentric ring represents one isolate, with ring position from inner to outer corresponding to individual isolates in the dataset. Colour intensity within each ring indicates the degree of nucleotide sequence identity to the reference genome at each genomic position, where fully coloured regions represent high sequence similarity and white/absent regions indicate low similarity, deletions, or genomic regions absent in that isolate relative to the reference. The genomic coordinate scale (in kilobase pairs, kbp) is displayed along the innermost reference ring. The GC content and GC skew tracks are shown as the innermost black waveform rings

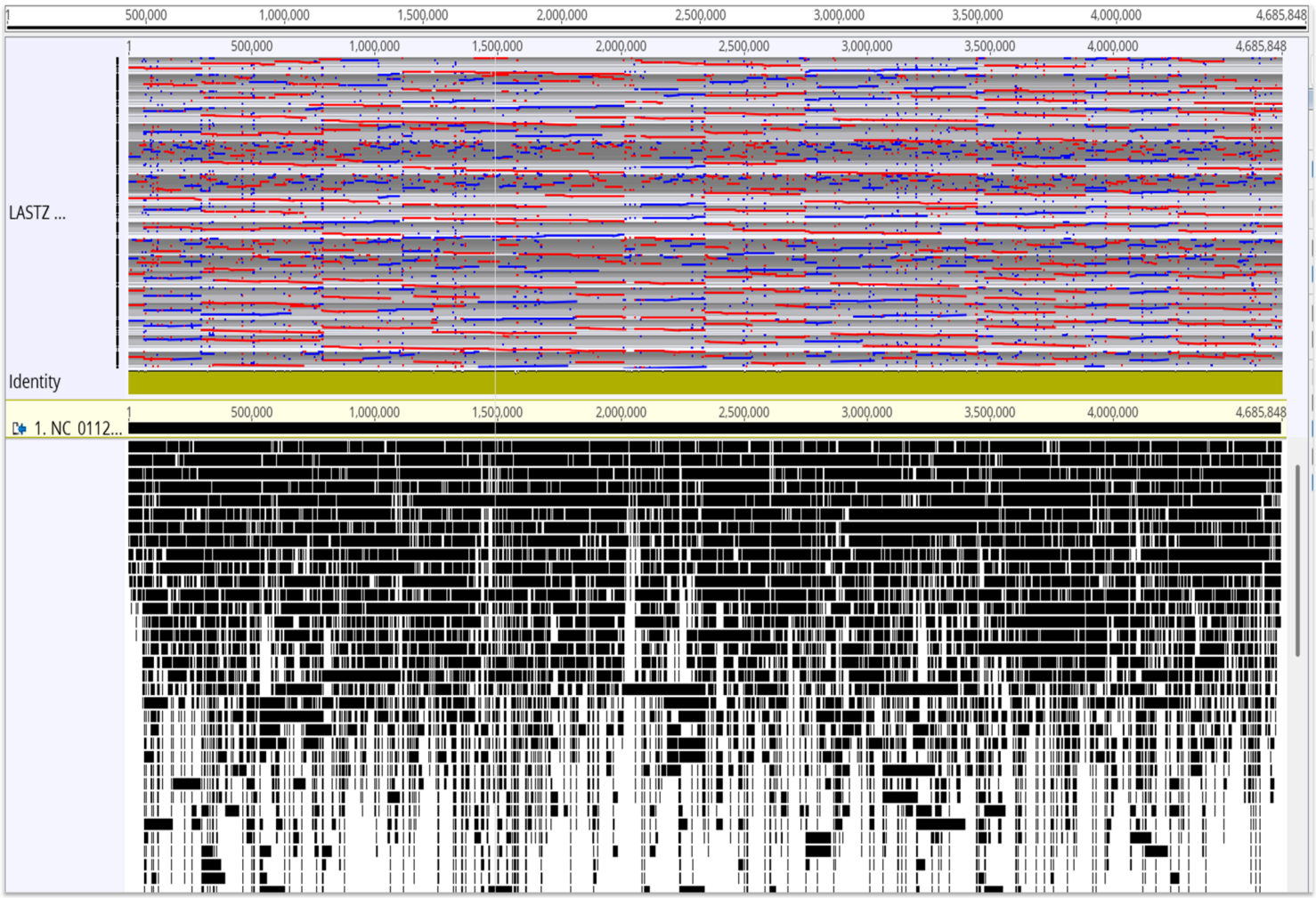


Figure 9

Whole-genome pairwise alignment of Salmonella enterica African isolates against the reference genome NC_011294 visualised in Geneious.

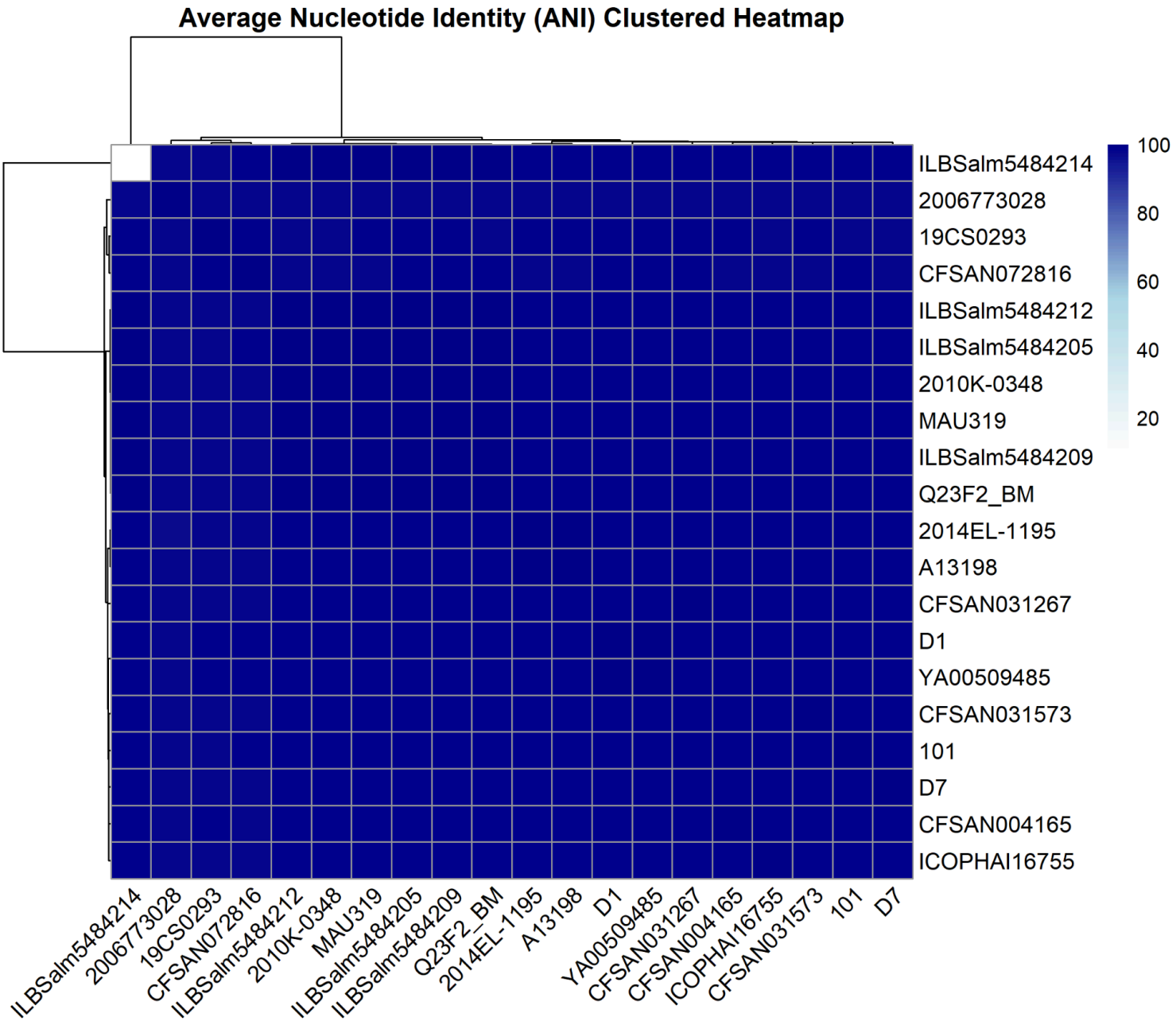


Figure 10

Pairwise Average Nucleotide Identity (ANI) heatmap of African Salmonella enterica isolates. The heatmap displays pairwise ANIb values calculated between 20 Salmonella enterica isolates using pyANI, with hierarchical clustering (complete linkage) applied along both axes. Each cell represents the ANIb value between two isolates encoded on a white-to-dark-blue scale (20–100%). The matrix is almost entirely dark blue, indicating uniformly high ANIb values (~98–100%) across nearly all isolate pairs, confirming intraspecific classification well above the 95% species boundary. The sole exception is the white cell pair corresponding to ILBSalm5484214 and 2006773028, representing the lowest ANIb value in the dataset. This divergence is reflected in the dendrogram topology, where ILBSalm5484214 forms a separate branch distinct from all other isolates. Diagonal cells represent self-comparisons at 100% identity.